Covalent bonding and bandgap formation in intermetallic compounds: a case study for Al_3V

2002 J. Phys.: Condens. Matter 14 1865

(http://iopscience.iop.org/0953-8984/14/8/314)

INSTITUTE OF PHYSICS PUBLISHING JOURNAL OF PHYSICS: CONDENSED MATTER

J. Phys.: Condens. Matter **14** (2002) 1865–1879 PII: S0953-8984(02)30309-6

Covalent bonding and bandgap formation in intermetallic compounds: a case study for Al_3V

M Krajčí[1,2] **and J Hafner**[1]

[1] Institut für Materialphysik and Center for Computational Materials Science, Universität Wien, Sensengasse 8/12, A-1090 Wien, Austria
[2] Institute of Physics, Slovak Academy of Sciences, Dúbravská cesta 9, SK 84228 Bratislava, Slovakia

Received 2 November 2001
Published 15 February 2002
Online at stacks.iop.org/JPhysCM/14/1865

Abstract

We demonstrate that a special hybridization between the Al(s, p) and V(d) orbitals which is responsible for forming of a deep pseudogap near the Fermi level in the Al_3V compound is also associated with the formation of covalent bonds. We analyse the charge distribution in the elementary cell and find an enhanced charge density along the Al–V bonds and certain Al–Al bonds which is characteristic for covalent bonding. The role of the point-group symmetry and the character of the hybrid orbitals forming the covalent bonds are investigated. It is demonstrated that the deep pseudogap close to the Fermi level arises from the bonding–antibonding of the hybrid orbitals.

1. Introduction

Alloys composed of metallic elements are naturally expected to be metallic too. However, in intermetallic compounds formed by transition metals (TMs) and polyvalent main-group elements such a Al or Si, in some cases hybridization can lead to the formation of a bandgap at or close to the Fermi level and eventually even semiconducting behaviour. Prototypes of such semiconducting or semimetallic compounds are certain refractory disilicides with the orthorhombic C54 ($TiSi_2$), C40 ($CrSi_2$) or $C11_b$ ($MoSi_2$) structures. Density-functional calculations [1–3] led to excellent predictions of the structural and electronic properties, but also demonstrated a high degree of sensitivity of the calculated gap to the local TM–Si coordination geometry. More intriguing are the results for the monosilicide FeSi, where the temperature dependence of the susceptibility and resistivity [4–7] shares certain features with a class of rare-earth compounds known as hybridization-gap semiconductors or Kondo insulators [8, 9].

Less well known are the properties of TM aluminides showing similar properties. $RuAl_2$ (which crystallizes in the $TiSi_2$ structure) shows infrared activity [10] and calculations have confirmed the existence of a bandgap [11]. Even more exciting are the properties of the homologous compound $FeAl_2$. Unlike $RuAl_2$ and $OsAl_2$, $FeAl_2$ crystallizes neither in the $MoSi_2$ structure (adopted by $OsAl_2$ and the low-temperature phase of $RuAl_2$)

nor the $TiSi_2$ structure, but in a complex triclinic structure [12]. At low temperatures, spin-glass behaviour has been reported [13], and entropy effects are thought to be responsible for stabilizing the triclinic lattice. Trialuminides with the DO_{22} structure have been studied extensively: they show high-temperature strength and excellent oxidation resistance, but their potential use as structural materials is severely limited by their poor ductility, which may be improved if the tetragonal DO_{22} structure may be changed to the cubic $L1_2$ phase. Band-structure calculations [14–17] have shown that the total density of states (DOS) of these compounds exhibits a deep minimum in the vicinity of the Fermi level which has been attributed to a hybridization between the Al-p and TM-d states. Out of this class of alloys, Al_3V shows the most interesting properties [18–21]: the temperature dependence of the electrical resistivity and the susceptibility show, like those of FeSi, a certain resemblance with heavy-fermion systems. A significant feature of the electronic spectrum of the Al_3V compound revealed by the electronic structure calculations [11, 16] is a very deep pseudogap in the DOS close to the Fermi level, indicating that Al-p/TM-d hybridization effects are particularly strong in this material.

The physical properties of dilute TM aluminides are often discussed in the framework of Friedel–Anderson virtual-bound-states (VBSs) model [22, 23]. In this model the TM atoms are far apart compared with the radius of the d-orbital, so d–d overlap is very small. A much stronger interaction arises from the mixing of d-states with conduction band of surrounding free-electron atoms, and their hybridization leads to the formation a VBS. The VBS has the nature of a resonance at the Fermi level because it is rather narrow ($\approx$1 eV) compared with the characteristic width of the d-band of pure metal ($\approx$5 eV). In the DOS the VBS creates an asymmetric narrow peak, followed by a minimum which is often referred to as the hybridization gap. In the Al_3V compound the transition atoms are not nearest neighbours and hence VBS model might apply. However, specific heat and resistivities measurements [19] suggest that although the VBS model may apply for many of aluminium-rich Al–TM metal phases, for the description of the anomalous properties of the Al–V compounds the VBS model fails [19].

An alternative framework is provided by the Hume–Rothery rule [24, 25]. It is based on a free-electron picture and correlates the structure and the average number of electrons per atom. If the conduction electrons may be described as free-electron like and the number of electrons per atom is such that the Fermi surface touches the Brillouin zone then the DOS around the Fermi level is reduced in comparison with the free-electron value by the formation of a structure-induced gap or pseudogap. The condition for formation of the pseudogap is as $2k_F \approx K_l$, where k_F is the momentum of electrons at the Fermi level and $\vec{K}_l$ represent the reciprocal vectors that correspond to the Brillouin zone. The formation of a pseudogap at the Fermi level can result in anomalous physical properties, e.g. low values of electronic specific heat (0.25 mJ mole^{-1} K^{-2} for icosahedral AlPdMn [31]).

While the Hume–Rothery argument has been successfully used for the explanation of the stability of alloys of the noble metals with polyvalent simple metals (known as Hume–Rothery alloys) and in attempts to explain the observed anomalous physical properties of quasicrystalline alloys of Al with elements with a full d-band (e.g. AlMgZn, AlCuLi) [26–30], its application to quasicrystalline Al–TM alloys such as AlPdMn or AlPdRe is less convincing. While the broad minimum found in the Al-DOS might be structure induced, the very narrow and sharply confined gap in the TM-bands cannot be attributed to a Hume–Rothery mechanism. The same applies to Al_3V where the simultaneous observation of a relatively high electronic specific heat of Al_3V (indicating a substantial DOS at the Fermi level) and of transport properties characteristic for a gap in the excitation spectrum, together with recent NMR studies of the trialuminide intermetallics [20] indicating strong directional bonding in these alloys suggest that the free-electron picture is not applicable.

This paper is part of a comprehensive study of the electronic properties of Al-rich Al–TM alloys. Here we present the Al_3V system. For this system we shall demonstrate that the correlation between covalent bonding effects and the formation of a gap at the Fermi level can eventually lead to non-metallic properties. Future work will be devoted to the exploration of the structural and electronic criteria for gap formation in a wide range of compounds.

The Al_3V compound has the DO_{22} (Al_3Ti) crystal structure. This is a modified face-centred cubic (fcc) structure. The crystal symmetry may be relevant for the origin of the deep pseudogap in the DOS. The pseudogap may be influenced also by the point-group symmetry of a particular atomic site. The well known e_g–t_{2g} splitting of d-orbitals in a local field with O_h point-group symmetry can be relevant, although the vanadium site in Al_3V has a distorted octahedral nearest-neighbour environment and the site-symmetry is reduced to D_{4h}. In order to discuss the effect of symmetry on the electronic structure we studied Al_3V also in the $L1_2$ (Cu_3Au) crystal structure. This structure is also a modified fcc structure, but the point-group symmetry O_h of the vanadium site is here not broken.

In this paper we shall demonstrate that the hybridization between Al(s, p) and V(d) orbitals leads to the formation of strong covalent Al–V bonds and also to a covalency of certain Al–Al bonds. In section 5 we analysed charge distribution in the elementary cell and found enhanced charge density along Al–V bonds and some Al–Al bonds which is characteristic for covalent bonding. In section 6 the role of symmetry and the mechanism of bonding is studied.

2. Methodology

The electronic structure calculations have been performed using two different techniques: the plane-wave based Vienna *ab initio* simulation package VASP [35, 36] has been used for the calculations of the electronic ground state and for the optimization of the atomic volume and unit-cell geometry of Al_3V in the $L1_2$ and DO_{22} structure. However, a plane-wave based approach such as VASP produces only the Bloch states and the total DOS, a decomposition into local orbitals and local orbital-projected DOSs requiring additional assumptions. To achieve this decomposition, self-consistent electronic structure calculations have been performed using the tight-binding linear muffin-tin orbital (TB-LMTO) method [32–34]. The LMTO basis includes s, p, and d orbitals for each of the Al and V atoms. In some calculations, see Sec 6, we included also f orbitals on V atoms. The two-centre TB-LMTO Hamiltonian has been constructed and diagonalized using the standard diagonalization techniques. The VASP program has also been used to calculate charge distributions. In its projector-augmented-wave (PAW) version [36] VASP calculates the exact all-electron eigenstates, hence it produces more realistic electron densities than those derived from muffin-tin-orbitals. The total DOS, band structures and total energies produced by both techniques are found to be in good agreement.

3. Crystal structure

3.1. Al_3V in the DO_{22} crystal structure

Al_3V is an intermetallic compound with a DO_{22} (Al_3Ti) crystal structure. The space group is $I4/mmm$ (No 139). The primitive cell contains four atoms. The orthorhombic elementary cell consists of two primitive cells, see figure 1(*a*). All atoms are located on the sites of a fcc lattice. The elementary cell consists of two fcc unit stacked along the z-direction. In the $z = 0$ plane the vertices of the cubic lattice are occupied by vanadium atoms and the face centres by aluminium atoms. In the $z = 0.5$ plane the arrangement is just the opposite. The planes $z = 0.25$ and 0.75 are occupied by aluminium atoms only.

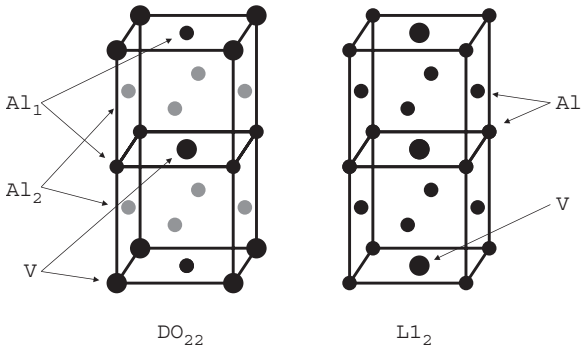

Figure 1. An elementary cell of Al_3V in the DO_{22} structure (*a*) and two elementary cells of Al_3V in the metastable $L1_2$ structure (*b*). Positions of aluminium atoms are represented by smaller circles, position of vanadium atoms are represented by bigger circles.

In order to be able to compare the properties of Al_3V in the DO_{22} crystal structure with the metastable $L1_2$ structure described below the atomic coordinates were determined not only from the crystallographic data [37] but also by selfconsistent total-energy calculations. The structure was relaxed using the VASP program [35, 36]. The lattice parameter obtained by the relaxation was $a = 3.764$ Å, i.e. slightly higher than that from crystallographic data, $a = 3.72$ Å. We note that such higher values are characteristic for all density functional calculations performed in the generalized gradient approximation (GGA). The equilibrium value of the axial ratio calculated in the GGA is $c/a = 2.207$, in very good agreement with the measured axial ratio of $c/a = 2.202$. The Al–V and Al–Al interatomic distances presented below and further in this paper refer to the geometry obtained by the VASP program.

In the elementary cell there are one vanadium crystallographic site V (Wyckoff notation 2a) and two aluminium sites Al_1 (2b) and Al_2 (4d). Each vanadium atom has four Al_1 neighbours and eight Al_2 neighbours. Al_1 neighbours are located in (x, y) plane at $z = 0$ and 0.5 on vertices of a square centred by the V atom. The distance between the central V atom and the Al_1 atoms is $d_{V-Al_1} = 2.661$ Å. Al_2 neighbours are located in $z = 0.25$ and 0.75 planes in vertices of a tetragonal prism centred again by the V atom at a distance $d_{V-Al_2} = 2.802$ Å. Considering only nearest neighbours the point-group symmetry of the V-site would be O_h, but nonequivalent neighbours from the second and higher shells reduce the point-group symmetry to D_{4h}.

An Al_1 atom sees four vanadium atoms located at $d_{Al_1-V} = 2.661$ Å on the vertices of a square and eight Al_2 neighbours located at $d_{Al_1-Al_2} = 2.802$ Å forming a tetragonal prism centred by the Al_1 atom.

Al_2 has four Al_2 atoms in the (x, y) plane forming together a square grid of aluminium atoms. The edge of the squares measures 2.661 Å. Al_2 has also four Al_1 and four V neighbours, both with tetrahedral coordination at a distance of 2.802 Å.

In summary, the vanadium atom has 12 aluminium nearest neighbours, both aluminium atoms have four vanadium neighbours and eight aluminium neighbours in the first coordination shell.

3.2. Al_3V in $L1_2$ crystal structure

The $L1_2$ (Cu_3Au) crystal structure is similar to the DO_{22} structure, but its symmetry is higher. The space group is $Pm3m$ (no 221), all atoms are located on the sites of fcc, see figure 1(*b*). Vanadium atoms are located in the vertices of cubic lattice, aluminium atoms

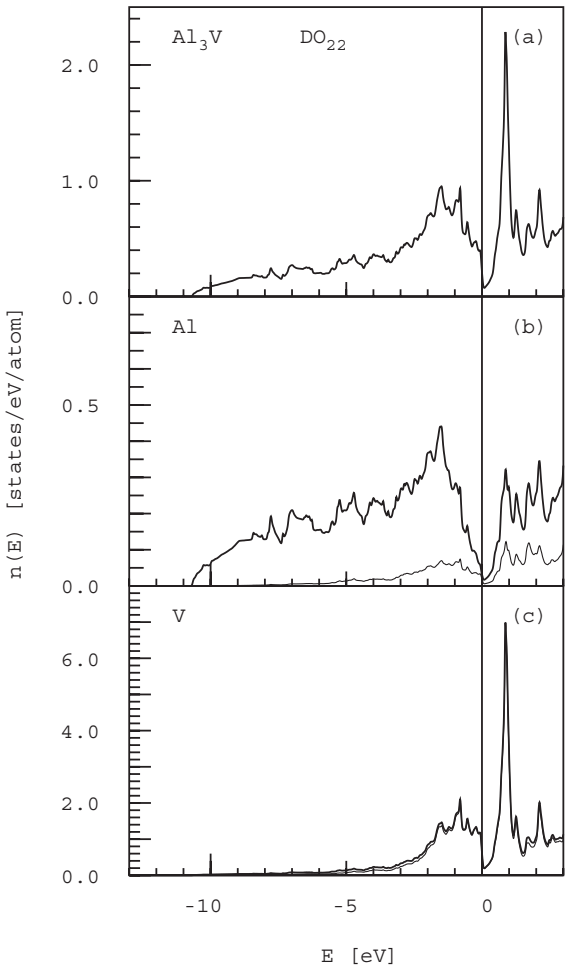

Figure 2. The DOS of Al_3V in the DO_{22} structure. Total DOS (*a*) and partial aluminium DOS (*b*) and vanadium DOS (*c*). Thin curve represents the contribution from d electrons.

occupy the face centres. In contrast to the DO_{22} structure there is only one Al site (3c) and one V site (1a). The lattice parameter obtained by VASP ($a = 3.896$ Å) is 3.5% larger than in the DO_{22} structure which implies also a larger Al–V distance of 2.755 Å in the $z = 0$ plane. An aluminium atom has 12 nearest neighbours, eight aluminium and four vanadium. A vanadium atom has 12 equivalent aluminium nearest neighbours. The total number of nearest neighbours around aluminium and vanadium atoms is thus the same as in the DO_{22} structure. A notable difference between both structures is that all nearest-neighbour Al–V and Al–Al distances are the same ($d_1 = 2.755$ Å) and that the point-group symmetry of the V site is exactly O_h.

The comparison of the total energies calculated by the VASP program $E_{tot}(DO_{22}) = -5.286\,21$ eV/atom, $E_{tot}(L1_2) = -5.148\,49$ eV/atom shows that the DO_{22} structure has the lower energy, in agreement with experiment. These values could be compared with the total energies of the pure elements in their ground-state structures: the total energy of Al in the fcc (A1) structure is $E_{tot}(A1) = -3.693\,33$ eV/atom. The total energy of V in the bcc (A2) structure is $E_{tot}(A2) = -8.935\,22$ eV/atom. A linear interpolation of these values for Al_3V composition gives $-5.003\,80$ eV/atom.

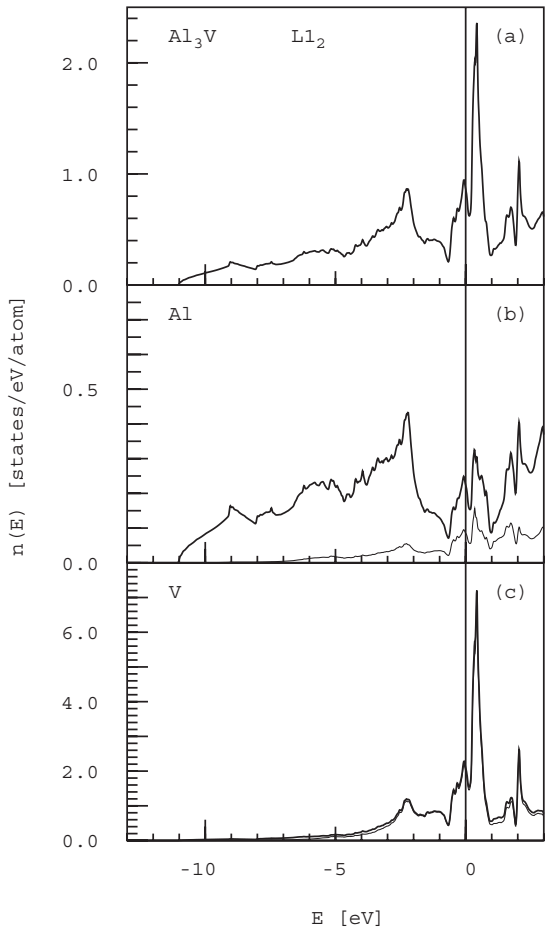

Figure 3. The DOS of Al_3V in the $L1_2$ structure. Total DOS (*a*) and partial aluminium DOS (*b*) and vanadium DOS (*c*). Thin curve represents contribution from d electrons.

4. Electronic structure

The electronic structure of Al–TM systems typically exhibits a narrow TM d-band superposed on a parabolic-like Al band. The total DOS is more or less modulated by van Hove singularities, bonding–antibonding d-band splitting and possible hybridization effects. For transition metals the Fermi level is located in a region of high DOS, which results in characteristic metallic properties of the system.

The electronic structure of the Al_3V has been already calculated by other authors [11, 16]. Concerning the form of the DOS our results confirm the findings of the previous calculations. The DOS is dominated by a deep pseudogap very close to the Fermi level. Figure 2 displays the total DOS of Al_3V with its orbital contributions and partial Al and V DOS.

The calculated DOS $n(E_F)$ reported by Trambly *et al* [11] is $n(E_F) = 0.13$ states/eV/atom. This low value of DOS at the Fermi level is significantly lower than the value of $n(E_F)$ for fcc Al, $n(E_F) \approx 0.37$ states/eV/atom. Our value is somewhat higher, $n(E_F) = 0.18$ states/eV/atom. The Fermi level is located at the steeply descending part of the pseudogap. The value of $n(E)$ in the minimum of the pseudogap (which is only 0.15 eV above the E_F) is extremely low $n(E_F) = 0.04$ states/eV/atom. On the other hand, the low

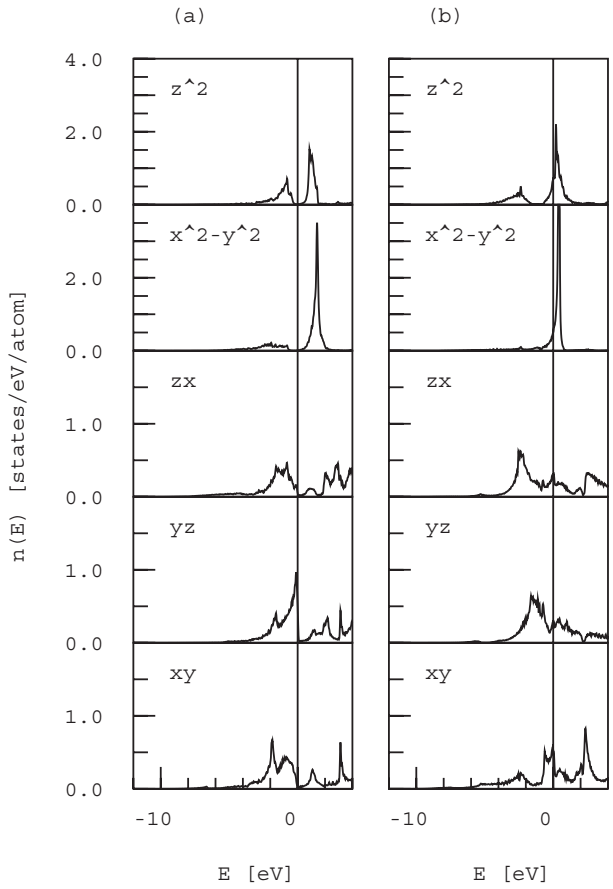

Figure 4. Orbital decomposed d-electron DOS of Al_3V in the DO_{22} (*a*) and $L1_2$ (*b*) structures. From bottom to top: d_{xy}, d_{yz}, d_{zx}, $d_{x^2-y^2}$ and d_{z^2}.

value of DOS at the Fermi level is not confirmed by the electronic specific heat measurements. The value of low-temperature specific heat $\gamma \approx 1.48$ mJ mole^{-1} K^{-2} (per mole of average atom) reported from experimental measurements [19] is quite close to the value 1.38 for fcc Al. However, even a very small change in the stoichiometry can lead to a substantial increase of the calculated DOS.

The DOS of Al_3V in the $L1_2$ structure is shown in figure 3. A broad DOS minimum is found at $E = -0.85$ eV, resulting from a clear splitting of the vanadium d-band. Figures 4(*a*), (*b*) shows the orbital-decomposed densities of states of the vanadium atom for both crystal structures, it reveals that the origin of d-band splitting in the $L1_2$ structure is e_g–t_{2g} splitting of d-orbitals in a local field with O_h point-group symmetry. The orbitals $d_{x^2-y^2}$ and d_{z^2} with e_g symmetry form a sharp peak ∼0.5 eV above the Fermi level. The peak of DOS at ∼2.5 eV is formed dominantly by orbitals with t_{2g} symmetry. The d-orbital splitting in the $L1_2$ structure (∼3 eV) is larger than in the DO_{22} structure (∼2.5 eV).

Comparison of the electronic structure of Al_3V for both crystal structures demonstrates that the symmetry splitting of d-orbitals is not fundamentally different in both structures, although the symmetry of the V-sites is reduced in the DO_{22} structure. The decisive difference determining the existence/absence of a deep pseudogap at E_F evidently arises from a different degree of hybridization of the V–t_{2g} ($d_{xy}\ldots$) states with the Al s, p states.

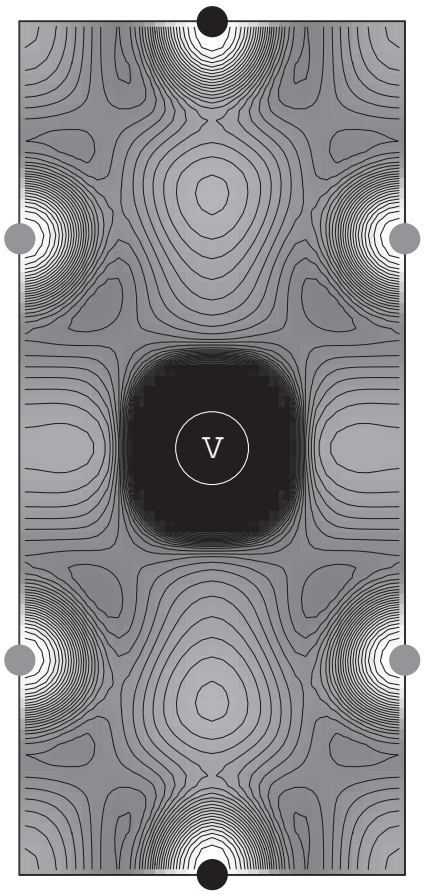

Figure 5. Contour plot of valence electron density in the (x, z) plane of the DO_{22} structure for $y = 0.5$. High charge density in the centre—the dark region—corresponds to the vanadium atom. The positions of the aluminium atoms are characterized by minima of charge density—light regions. The islands of enhanced charge between the central V atom and four Al_2 atoms indicate possible covalent bonding.

5. Charge densities and bonding

Using the VASP program we calculated the charge-density distribution in the elementary cell of the DO_{22} structure. Figure 5 shows a contour plot of the valence-charge distribution in the (x, z) plane for $y = 0.5$. The high charge-density in the centre (dark region) corresponds to the vanadium atom. The positions of aluminium atoms are characterized by minimal charge densities—light regions. If the character of the bonding is purely metallic, the charge distribution among atoms should be homogenous. A possible covalent bonding is indicated by enhanced charge distribution along connections between atoms. In figure 5 we see regions of enhanced charge-density halfway between the central V atom and four Al_2 atoms. As the structure has tetragonal D_{4h} symmetry around the z-axis the same distribution exists also in the perpendicular (y, z) plane.

To confirm the covalent bonding we investigated the difference electron density, i.e. a superposition of atomic charge densities is subtracted from the total charge density.

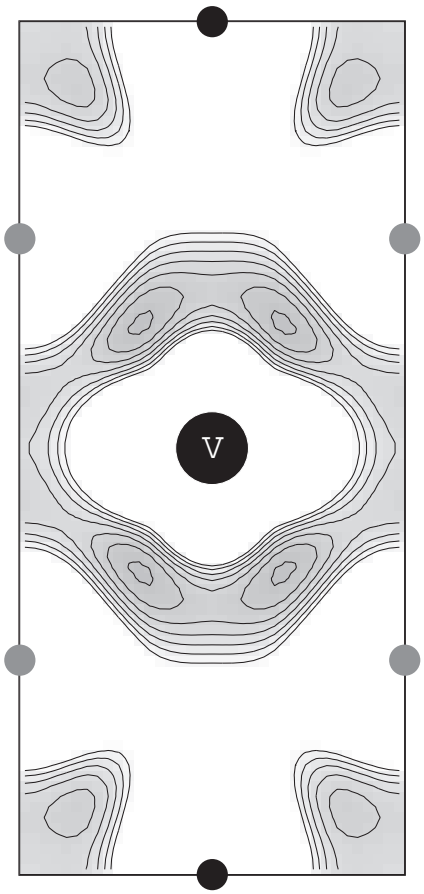

Figure 6. Contour plot of the difference electron density in the (x, z) plane for $y = 0.5$ (the same plane as in the previous figure). In the difference density a non-selfconsistent charge density obtained as a superposition of atomic charge densities is subtracted from the total charge density. In the figure we represent only regions of enhanced density. In blank regions among atoms the difference density is negative. One can clearly identify enhanced charge corresponding to bonding between the V atom and Al_2 atoms.

The contour plot in figure 6 represents the regions of positive difference electron density in the (x, z)-plane, in the blank space the difference density is negative. In figure 6 we can clearly identify the 'bond charges' between the V and Al_2 atoms. The bonds are directed from the central vanadium atom to the eight vertices of a tetragonal prism formed by the Al_2 atoms. A similar bonding was found between the V and Al_1 atoms. Figure 7 shows a contour plot of the difference electron density in the (x, y) plane at $z = 0$. The bonds are directed from the central vanadium atom to the four vertices of a square formed by the Al_1 atoms. An enhanced charge density was found also in the planes at $z = 0.25$ and 0.75 where only Al_2 atoms are located, see figure 8. In summary, there are three types of covalent bonds. The bonds are sketched in figure 9: the vanadium atom has two types of bonds: V–Al_2 bonds are marked as dashed lines, V–Al_1 bonds are displayed as dash–dotted line segments. The Al_2 atoms have, in addition to the bonds with the V atom, Al_2–Al_2 bonds marked in figure 9 by dotted lines. The character of the bonds is investigated in the next section.

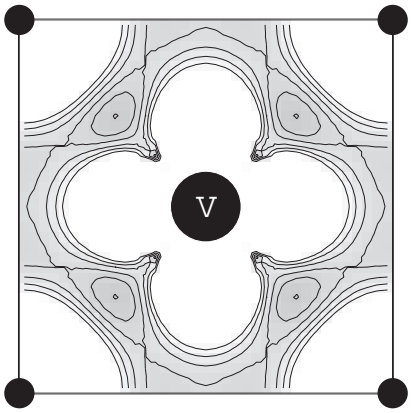

Figure 7. Contour plot of difference electron density in the (x, y) plane for $z = 0$. One can clearly identify enhanced charge corresponding to bonding between the V and Al_1 atoms.

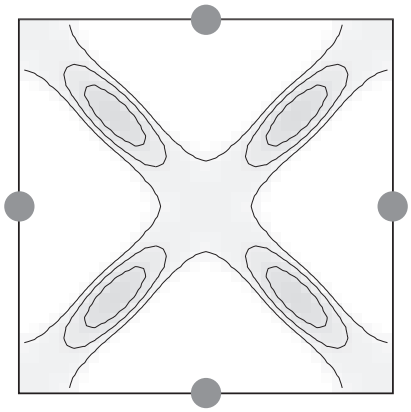

Figure 8. Contour plot of difference electron density in the (x, y) plane for $z = 0.25$. One can clearly identify enhanced charge corresponding to bonding between Al_2 atoms.

6. Hybridized orbitals and bonding

Bonding in an intermetallic compound can be very complex. Fortunately, in the DO_{22} crystal structure where the symmetries of atomic sites are relatively high, symmetry can help to identify the orbitals or hybridized orbitals that are most important for forming the bonds. To gain a deeper understanding, we constructed sets of symmetrized hybridized orbitals oriented along the bonds and calculated the DOS projected onto bonding and antibonding combinations of these symmetrized orbitals.

6.1. Symmetrized orbital sets

The symmetrized orbitals are sets of hybridized orbitals possessing the point-group symmetry of a particular atomic site. Here we shall investigate σ-bonds only. A set of σ-bonds originating from a particular atom forms a reducible representation of the point group [38]. Decomposition of the reducible representation into irreducible ones enables one to select individual s, p or d orbitals whose linear combinations form the hybridized orbitals.

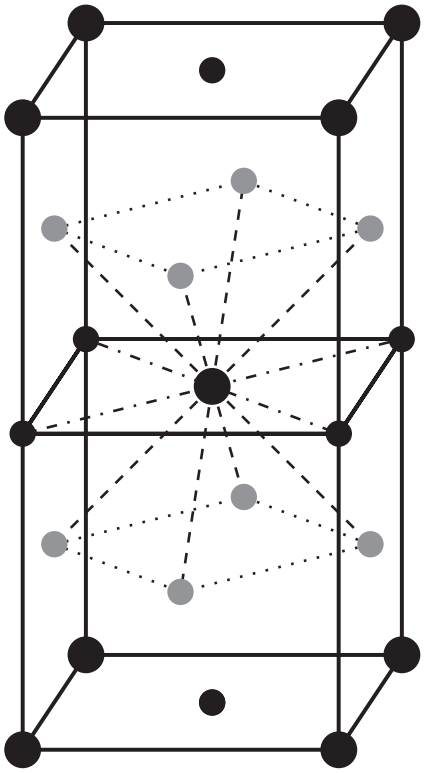

Figure 9. An elementary cell of Al_3V in the DO_{22} structure. The positions of the aluminium atoms are represented by smaller circles and the positions of the vanadium atoms are represented by larger circles. Three types of covalent bonds are sketched: V–Al_2 bonds are marked as dashed lines, V–Al_1 bonds are displayed as dash–dotted lines, Al_2–Al_2 bonds are marked in by dotted line segments.

6.1.1. Al_2–Al_2 bonds. Each Al_2 atom has four Al_2 neighbours located at the vertices of a square. The symmetrized orbitals correspond to sp^2d hybridization. As we have seen in figure 2, the d-states contribution to the aluminium DOS is not negligible and therefore including an $Al_2(d_{xy})$ orbital into the hybridized set describing the Al_2–Al_2 bonding is legitimate. The symmetrized orbitals $\phi_1 \ldots \phi_4$ are constructed as a linear combination of s, p_x, p_y and d_{xy} orbitals.

6.1.2. V–Al_1 bonds. There are two sets of hybridized orbitals—one on the aluminium atoms and the other on the vanadium atom:

(i) The Al_1 atoms have four V neighbours located at the vertices of a square. The corresponding set of symmetrized hybridized orbitals is again sp^2d with Al_1 s, p_x, p_y and d_{xy} orbitals.

(ii) From the point of view of the vanadium atom the V–Al_1 bonds are oriented from the central V atom to four Al_1 atoms located at the vertices of a square. The corresponding set of symmetrized orbitals is again sp^2d. However, as the contribution of p-states to the vanadium DOS is negligible and the contribution of s-states is small, the V(d_{xy}) orbital is dominant.

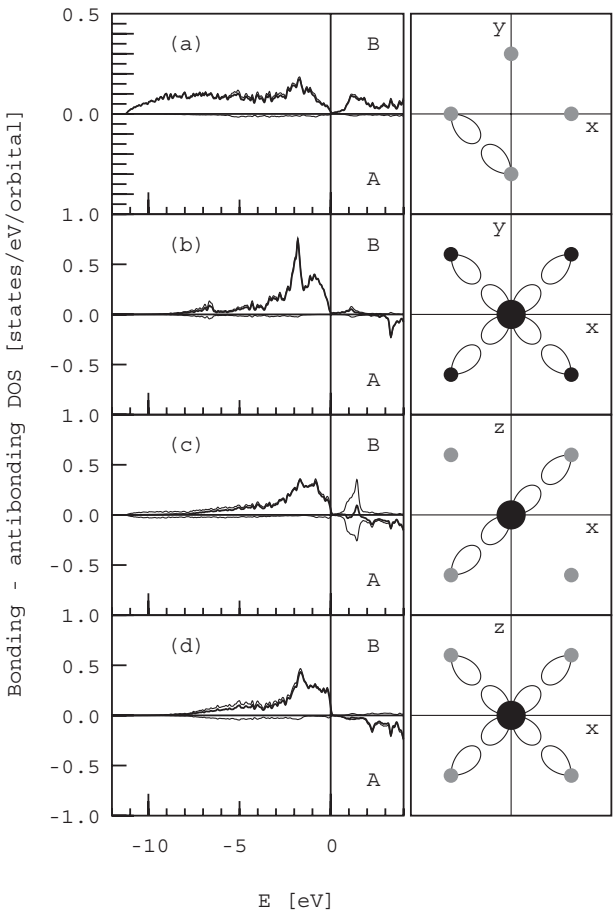

Figure 10. The crystal-orbital overlap population (coop). The DOS is projected on a bonding (B) and antibonding (A) combination of symmetrized orbitals located on atoms. In addition to the bonding density and antibonding density which, for the sake of clarity a negative sign is assigned (both thin lines) the difference (B–A) between bonding and antibonding densities is presented (thick line). (*a*) $Al_2(sp^2d)$–$Al_2(sp^2d)$ bonding, (*b*) $V(d_{xy})$–$Al_1(sp^2d)$ bonding, (*c*) $V(d^4)$–$Al_2(sp^3)$ bonding, and (*d*) $V(d_{zx}, d_{yz})$–$Al_2(sp^3)$ bonding. The orbitals participating in the bonding are schematically presented in the right panel.

6.1.3. V–Al_2 bonds.

(i) The Al_2 atoms have four V neighbours located at the vertices of a tetrahedron. The symmetrized orbitals on the Al_2 atoms are thus sp^3 hybrids formed by s, p_x, p_y and p_z orbitals.

(ii) The point group symmetry of the vanadium site is D_{4h}. The orbitals oriented from the central vanadium atom to the eight Al_2 atoms at the vertices of a tetragonal prism form a basis of a reducible representation of the D_{4h} point group. Reduction yields four one-dimensional representations A_{1g}, A_{2u}, B_{1g}, B_{2u} and two two-dimensional representations E_g and E_u. The assignment of atomic orbitals to irreducible representations with the same transformation properties is the following: A_{1g}: s or d_{z^2}, A_{2u}: p_z, B_{1g}: $d_{x^2-y^2}$, B_{2u}: $f_{z(x^2-y^2)}$, E_g: (d_{zx}, d_{yz}), E_u: (p_x, p_y), leading to sp^3d^3f or p^3d^4f hybrid orbitals on the vanadium atom. As already noted above the contribution of s-states to the vanadium DOS

is small and the contribution of p-states is negligible. We verified by a direct calculation that the same holds also for f-states. Therefore d^4 hybrid orbitals formed by the d_{z^2}, $d_{x^2-y^2}$, d_{zx}, d_{yz} states (or sd^3 hybridization if we consider the s orbital instead of the d_{z^2}) dominate the bonding. It is remarkable that the symmetry here excludes the d_{xy} orbital from bonding. This is the orbital which plays a dominant role in V–Al_1 bonding as discussed in the previous section.

It is also important to emphasize that mostly orbitals with even orbital quantum number l: d ($l = 2$) or s ($l = 0$) contribute to the hybridized orbitals on vanadium atom which therefore have inversion symmetry. Skipping p and f orbitals from the p^3d^4f hybrids we obtain instead of eight symmetrized orbitals pointing towards the vertices of a tetragonal prism four d^4 hybridized orbitals possessing inversion symmetry. The symmetrized d^4 orbitals have a form similar to the d_{z^2} orbital and differ only in orientation. While the d_{z^2} orbital is oriented along the z axis, the symmetrized d^4 orbitals are oriented along the body diagonals of the tetragonal prism.

6.2. Bonding and antibonding projected density of states

From the symmetrized orbitals we constructed bonding and antibonding configurations and investigated the DOS projected on these orbital configurations. (We note that the difference between these projected DOS is essentially equivalent to the differential crystal-orbital overlap population (coop) defined by Hoffmann [39].) Figure 10 shows the DOS projected on bonding (B) and antibonding (A) combinations of symmetrized orbitals located an neighbouring atoms. In addition to the bonding DOS and antibonding DOS (to which, for the sake of clarity, a negative sign is assigned), the difference (B–A) between bonding and antibonding densities (i.e. the coop; our definition differs from the original one by a factor of 2) is presented.

6.2.1. $Al_2(sp^2d)$–$Al_2(sp^2d)$ bonding. For the bonding between two Al_2 atoms in the (x, y) plane, (see the dotted lines in figure 9). The density of the antibonding configuration is negligibly small in the whole studied energy region (figure 10(*a*)), the coop is positive below and above the Fermi level, as well. This indicates that although the bond has a covalent character it is only partially populated by electrons. The minimum around the Fermi level does not have the character of a bonding–antibonding splitting, but is a consequence of a low total in this region induced by other bonding mechanisms.

6.2.2. $V(d_{xy})$–$Al_1(sp^2d)$ bonding. The vanadium atom interacts with four Al_1 atoms in the (x, y) plane, (see dot–dashed line segments in figure 9). Figure 10(*b*) shows that below the Fermi level the bonding DOS is substantially higher than the antibonding one. The region above the Fermi level up to 2.7 eV can be considered as nonbonding, both bonding and antibonding DOS are very close to zero. Above 2.7 eV the antibonding character becomes significant.

6.2.3. $V(d^4)$–$Al_2(sp^3)$ bonding. The vanadium atom is bonded with two Al_2 atoms located in opposite directions on the body diagonal of a tetragonal prism. Altogether there are four such bonds, see dashed lines in the figure 9. Figure 10(*c*) shows that while the bonding DOS below the Fermi level is substantial, the antibonding DOS is negligible in this region. At the Fermi level the bonding DOS decreases and above the Fermi level a nonbonding region extends to 1.5 eV. In this energy range a bonding contribution from the $d_{x^2-y^2}$ component, and an antibonding DOS from the d_{z^2} component largely compensate. Above $\sim$1.5 eV the antibonding character becomes dominant.

6.2.4. V(d_{zx},d_{yz})–Al$_2$(sp^3) bonding. A more detailed analysis of the V(d^4)–Al$_2$(sp^3) bonding shows that the main bonding contribution out of the four d^4 hybridized orbitals comes from the components d_{zx} and d_{yz} both belonging to the E_g irreducible representation. Figure 10(*d*) represents the bonding and antibonding densities corresponding to these states. Below the Fermi level (more exactly below 0.08 eV) the states have dominantly bonding character while above the Fermi level the character is antibonding. This demonstrates bonding–antibonding splitting of the energy levels and confirms the covalent character of the bond.

7. Discussion and conclusion

For Al_3V, NMR studies suggest a strong directional bonding [19,20]. This conjecture is further corroborated by the structural analysis: the unusually short Al–V distances [18] indicate that the bonding may have a covalent character. Our detailed investigation of the electronic structure of this compound confirms and extends these conjectures. Strong covalent bonding exists between the Al_2 atoms as well as between the V-atoms and both types of Al-atoms. The Al_2–Al_2 bonding is based on sp^2d hybrid orbitals. The interaction of the same hybrid orbitals on the Al_1-sites with the V-d_{xy} states forms the basis for the covalent Al_1–V bond. Al_2–V bonding is based on sp^3-hybrids on the Al-atoms and d^4-hybrids on the V-sites. The deep DOS-minimum just above the Fermi level originates from the bonding–antibonding splitting of these hybrid orbitals, as demonstrated by the calculation of the crystal-orbital overlap populations.

The strong covalent bonding also explains the mechanical properties of this compound, the localization of the electrons in the bonds provides also a qualitative explanation for the observed anomalies in the transport properties, although this deserves further investigation. Preliminary results indicate that the scenario for the formation of bandgaps in intermetallic compounds elaborated here has quite general validity, not only for crystalline, but also for quasicrystalline alloys.

Acknowledgments

This work has been supported by the Austrian Ministry for Science through the Center for Computational Materials Science. MK also acknowledges support from the Grant Agency for Science in Slovakia (Grant no 2/2038/22).

References

[1] Mattheis L F 1991 *Phys. Rev.* B **43** 1863
Mattheis L F 1991 *Phys. Rev.* B **43** 12 549
[2] Mattheis L F 1992 *Phys. Rev.* B **45** 3252
[3] Mattheis L F and Hamann D R 1993 *Phys. Rev.* B **47** 13 114
[4] Jaccarino V, Wertheim G K, Wernick J H, Walker L R and Arajs S 1967 *Phys. Rev.* **160** 476
[5] Schlesinger Z, Fisk Z, Zhang H T, Maple M B, DiTusa J F and Aeppli G 1993 *Phys. Rev. Lett.* **71** 1748
[6] Nyhus P, Cooper S L and Fisk Z 1995 *Phys. Rev.* B **51** 15 626
[7] Paschen P, Felder E, Chernikov M A, Degiori L, Schwer H, Ott H R, Young D P, Sarrao J L and Fisk Z 1997 *Phys. Rev.* B **56** 12 916
[8] Hundley M F, Canfield P C, Thompson J D and Fisk Z 1990 *Phys. Rev.* B **42** 6842
[9] Hundley M F, Canfield P C, Thompson J D and Fisk Z 1994 *Phys. Rev.* B **50** 18 142
[10] Basov D N, Pierce F S, Volkov P, Poon S J and Timusk T 1994 *Phys. Rev. Lett.* **73** 1865
[11] Trambly de Laissardière G, Nguyen Manh D, Magaud L, Julien J P, Cyrot-Lackmann F and Mayou D 1995 *Phys. Rev.* B **52** 7920
[12] Corby R N and Black P J 1973 *Acta Crystallogr.* B **29** 2669
[13] Lue C S, Öner Y, Naugle D G and Ross J H 2001 *Phys. Rev.* B **63** 184405

[14] Hong T, Watson-Yang T J, Freeman A J, Oguchi T and Xu J H 1990 *Phys. Rev.* B **41** 12 462
[15] Xu J H and Freeman A J 1990 *Phys. Rev.* B **41** 12 553
[16] Paxton A T and Pettifor D G 1992 *Scr. Metal.* **26** 592
[17] Weinert M and Watson R E 1998 *Phys. Rev.* B **58** 9732
[18] Caplin A D, Grüner G and Dunlop J B 1973 *Phys. Rev. Lett.* **30** 1138
[19] Dunlop J B, Grüner G and Caplin A D 1974 *J. Phys. F: Met. Phys.* **4** 2203
[20] Lue C-S, Chepin S, Chepin J and Ross J H Jr 1998 *Phys. Rev.* B **57** 7010
[21] Lue C-S and Ross J H Jr 1999 *Phys. Rev.* B **60** 8533
[22] Friedel J 1956 *Can. J. Phys.* **34** 1190
[23] Anderson P W 1961 *Phys. Rev.* **124** 41
[24] Hume–Rothery W 1926 *J. Inst. Met.* **35** 295
[25] Jones H 1937 *Proc. Phys. Soc.* **49** 250
[26] Mizutani U, Sakabe Y and Matsuda T 1990 *J. Phys.: Condens. Matter* **2** 6153
[27] Hafner J and Krajčí M 1992 *Phys. Rev. Lett.* **68** 2321
[28] Hafner J and Krajčí M 1993 *Phys. Rev.* B **47** 11 795
[29] Krajčí M, Hafner J and M. Mihalkovič 1996 *Europhys. Lett.* **34** 207
[30] Krajčí M, Hafner J and Mihalkovič M 1997 *Phys. Rev.* B **56** 3072
[31] Lasjaunias J C, Sulpice A, Keller N, Préjean J J and de Boissieu M 1995 *Phys. Rev.* B **52** 886
[32] Andersen O K 1975 *Phys. Rev.* B **12** 3060
Skriver H L 1984 *The LMTO Method* (Berlin: Springer)
[33] Andersen O K, Jepsen O and Götzel D 1985 *Highlights of Condensed Matter Theory* ed F Fumi and M P Tosi (New York: North-Holland)
[34] Andersen O K, Jepsen D and Šob M 1987 *Electronic Band Structure and its Applications* ed M Youssouff (Berlin: Springer)
[35] Kresse G and Furthmüller J 1996 *Comput. Mater. Sci.* **6** 15
Kresse G and Furthmüller J 1999 *Phys. Rev.* B **54** 11 160
[36] Kresse G and Joubert D 1999 *Phys. Rev.* B **59** 1758
[37] Villars P and Calvet L D 1991 *Pearson's Handbook of Crystallographic Data for Intermetallic Phases* vol 1 2nd edn (Materials Park, OH: American Society for Metals)
[38] Ballhausen C J and Gray H B 1965 *Molecular Orbital Theory* (New York: Benjamin)
[39] Hoffmann R 1988 *Solids and Surfaces: A Chemist's View of Bonding in Extended Structures* (New York: VCH)